京 都 大 学 防 災 研 究 所 年 報 第 48 号 C 平成 17 年
Annuals of Disas. Prev. Res. Inst., Kyoto Univ., No. 48 C, 2005

The Importance of Surface Heating in Short-term Numerical Weather Prediction

Kenji TANAKA, Kazuyoshi SOUMA*, Eiichi NAKAKITA,
and Shuichi IKEBUCHI
* Graduate School of Engineering, Kyoto University

Synopsis

In this study, six numerical experiments are carried out in mountainous region around the Lake Biwa on 14th and 15th August in 2001. These experiments are intended to see the importance of surface heating and soil moisture status for the formation of convective rain in the summer time. It is found that landcover condition and soil moisture condition can affect the amount of convective rain even in a very short-term prediction.

Keywords: landcover, soil moisture, local circulation, convective rain, short-term

1. Introduction

Many researches have been made in the past decade about the effect of land surface processes, especially soil moisture, on the middle to long-range weather prediction. Some of them are based on regional model (e.g. Kanae et al., 2001), and others are based on global model (e.g. Koster et al., 2004). Target of these researches is mainly soil moisture in the arid or semi-arid condition. And it has been recognized that soil moisture is strongly coupled with local climate in the semi-arid region.

On the other hand, the effects of land surface processes on the short-range weather prediction, especially in the humid climate condition, have not been discussed enough. Heating from land surface and intensity of local circulation can affect the transport of moisture and cumulous clouds. Some researches address the effect of topography to the transport of moisture and cumulous clouds (e.g. Kimura and Kuwagata, 1995). Shinoda et al.(2002) reported the importance of surface moisture flux (latent heat flux) from the paddy field on the formation of deep convection in the Meiyu front. However, the effects of land surface conditions (land cover, soil moisture) are still poorly understood.

In this study, the effect of surface heating is investigated with the mesoscale numerical weather prediction model ARPS (Advanced Regional Prediction System: Xue et al., 1995). To address the land surface conditions in detail, an advanced land surface scheme SiBUC (Simple Biosphere including Urban Canopy: Tanaka et al., 1998) is coupled into ARPS.

In the Lake Biwa Project, surface energy balance have been observed at three regular flux measurement sites, named paddy field, lake and forest sites, respectively (the locations are shown in Fig. 1). During the intensified field campaign of the Lake Biwa Project 2001, radiosonde observations were carried out near the paddy field

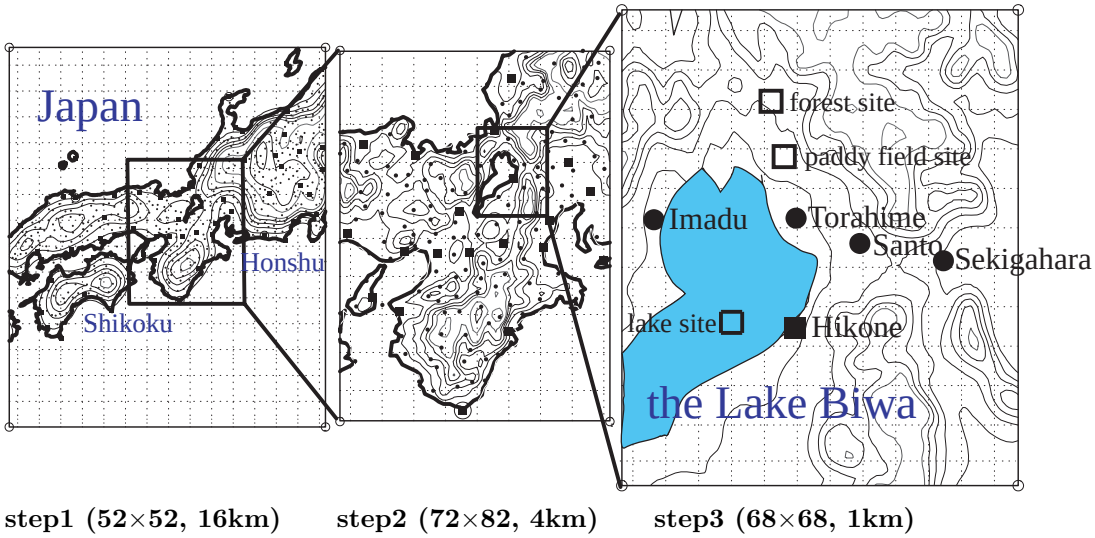

Fig. 1 Model domains and location of meteorological stations (Solid circles : AMeDAS observation sites, solid squares : surface observation sites, open circles : upper air observation sites, open squares : regular flux measurement sites of the Lake Biwa Project)

site. Well developed local circulation was observed on a typical summer sunny day (14th August 2001). This case is simulated with both the original ARPS (with simple land surface scheme) and the ARPS-SiBUC (with detailed land surface scheme). Through the comparison of the simulated values with observed values, the effects of urban area and subgrid scale land use mixture to the intensity of local circulation are discussed (Case1 and Case2). Furthermore, effect of surface heating is discussed by the land-cover change experiment (Case3 and Case4) and soil moisture change experiment (Case5 and Case6) for the simulation of thunderstorm event on 15th August 2001. Here, the comparison of Case3 and Case4 is to see the impact of land surface with a extreme condition such as replacing all forest to paddy field. On the other hand, the comparison of Case5 and Case6 is to see the importance of initial soil moisture within possible variation range.

Table 1 The list of numerical experiment

Case1	simple land surface scheme (ISBA)
Case2	detail land surface scheme (SiBUC)
Case3	landcover change (actual landuse)
Case4	landcover change (forest to paddy)
Case5	soil moisture change (wet)
Case6	soil moisture change (dry)

2. Description of the land surface scheme

The original ARPS has a relatively simple land surface scheme (LSS) based on ISBA (Interactions between the Soil Biosphere and Atmosphere: Noilhan et al., 1989). Only natural land surface areas such as forest, grassland and bare soil are considered in the LSS.

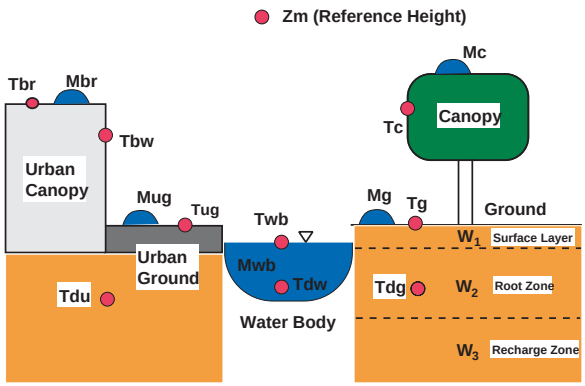

Fig. 2 Schematic image of surface elements in SiBUC

The SiBUC model uses mosaic approach to incorporate all kind of land-use into LSS, and it has been developed, validated, and applied mainly in Japan and China region. SiBUC has three submodels for green area(vegetation), urban area, and water body (see Fig. 2). The vegetation scheme is basically same as SiB (Simple Biosphere model:

Table 2 Model configuration

Dynamic Framework	Nonhydrostatic and fully compressible(3-D)
Coordinate System	Vertically-stretched terrain-following grid(43 layer) (Lowest level is 40m AGL. Model top is 16 km MSL) Rayleigh damping is applied to the upper 1/3 of the domain
Solution Technique	Mode-split with vertically-implicit option
Divergence Damping	divergence-damped Acoustic calculation
Top & Bottom Boundary Conditions	rigid wall
Lateral Boundary Conditions	externally-forced boundary conditions GPV from Regional Spectral Model(JMA)
Computational Mixing	4th-order
Advection	4th-order,simple positive definite scheme for water and TKE
Cloud Microphysics	3 ice-phase Microphysics(Lin-Tao)
Cumulus Parameterization	Kain-Fritsch(only for step1)
Subgrid Scale Turbulence	1.5-order turbulent kinetic energy formulation
PBL scheme	Convective PBL turbulence based on TKE scheme
Surface Layer	bulk aerodynamic drag laws with stability-dependent
Soil Model	1-layer Soil and Surface Energy Balance Model(ISBA) 11 Soil Categories, 13 Vegetation Categories
Longwave and Shortwave Radiation	Atmospheric Radiative Transfer
time step	step1:12sec, step2:5sec and step3:5sec, respectively

Sellers et al., 1986), but some simplification from original SiB was done. A Rice paddy field is so unique and specific since it can store plenty of water above soil surface. In the original version of SiB and most of the LSSs currently implemented in numerial weather prediction models and global climate models, there is no framework to treat rice paddy field properly. Therefore, paddy field scheme, which has water layer above soil surface, and which can treat artificial water irrigation/drainage was developed and implemented into green area model.

3. Experimental design

3.1 Configuration of atmospheric model

Two numerical experiments are performed for 12 hours from 03:00JST on 14th August during the intensified observation period of the Lake Biwa Project. The first experiment (Case1) is performed by the original ARPS coupled with the ISBA. The second experiment (Case2) is performed by the ARPS coupled with the SiBUC. The model configuration of the ARPS is shown in Table 2 and simulation domain is shown in Fig. 1.

The GPV (Grid Point Value) data of the RSM (Regional Spectral Model, a hydrostatic model used for operational forecast in Japan), which have about 40km resolution and 3-hour interval, are used as initial and boundary conditions for step1 simulation. The results of step1 is nested-down to step2 and step3 (one-way nesting). Upper air, surface observation and AMeDAS data are assimilated to produce realistic initial field by the ADAS (ARPS Data Assimilation System : Xue et al., 1995). The locations of observation stations are also shown in Fig. 1. And the result of the final domain with 1km mesh (step3) will be discussed.

3.2 Configuration of LSS

The fractional areas of land uses (urban area, water body and 10 category of green area) and canopy fraction within each land use are assigned to each grid. In this study, KS-202 data (with about 100m resolution and 15 land use categories) are reclassified into the land use fraction dataset with seven categories (paddy, farmland, grassland, mixed forest, bare soil, urban area, and water) and the reclassified dataset is used to calculate the fractional areas.

NDVI (Normalized Difference Vegetation Index) of Global AVHRR 10-day composite data (about 1km resolution) made by USGS (U.S. Geological Survey) are used to estimate the LAI (Leaf Area Index) in green areas.

As for soil type, a global digital soil map from FAO (Food and Agricultural Organization of the United Nations), which has about 10km resolution and more than 1000 categories is used. According to the detailed soil texture information for each soil type, this dataset is reclassified into 11 categories, such as sand and loamy sand.

Initial land-surface temperature is calculated from near-surface atmospheric temperature. As for initial sea-surface temperature, monthly averaged dataset of NOAA/NASA AVHRR Oceans Pathfinder SST is used, and it has about 9km resolution. As for initial lake-surface temperature of the Lake Biwa, the monthly averaged observation data at the lake site are used.

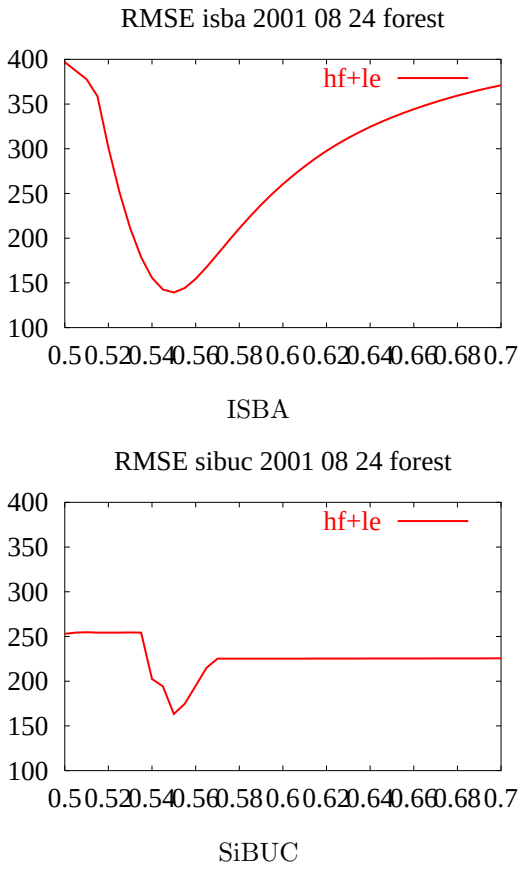

Fig. 3 Sum of the RMSE of sensible and latent heat flux on 24th August in offline simulations at the forest site

In order to define initial soil wetness, some offline simulations are carried out at the forest site. In the offline simulations with the ISBA and SiBUC models, the soil wetness is changed from 0.5 to 0.7 (shown in Fig. 3). Soil wetness is optimized so as to minimize the sum of RMSE of sensible and latent heat fluxes. Finally, initial soil wetness in forest area is defined as 0.55, and this value is used for Case1 through Case3. As for the grids classified as cultivation in the ISBA model, initial soil wetness is set to 1.0 (saturated), because basically all crops are identified as paddy field in the step3 domain.

4. Results and discussion (Case1 & Case2)

4.1 Surface flux

Fig. 4 through Fig. 6 show each term of surface energy balance equation ($R_n = Hf + lE + G$) at the paddy field, lake and forest sites. Observed data are processed by Bowen ratio method for paddy and forest, and by stability dependent Bulk method for lake, respectively. Here, the data for 24th August are used as reference data at forest site since the data for 14th August were missing.

In Fig. 4, the feature of observed energy balance at paddy field, that is, most of the net radiation is released as latent heat, is simulated very well by both Case1 and Case2. Although the SiBUC model has a specially designed paddy field scheme, the difference between the results of Case1 and Case2 does not seem to be much evident. This result was obtained by the treatment of soil moisture (saturated in initial condition) in ISBA. And the surface soil moisture does not decrease so much in the very short-term simulation.

In Fig. 5, net radiation simulated by Case1 is less than observed value. Diurnal variation of latent and sensible heat flux is simulated well by Case1 and Case2. This difference in net radiation does not seem to affect much on the local circulation.

In Fig. 6, simulated Bowen ratio is smaller (higher latent heat and lower sensible heat) than that of the reference values in both Case1 and Case2. The simulated surface fluxes are rather different from the reference values, however, the simulated flux by Case1 and Case2 are similar.

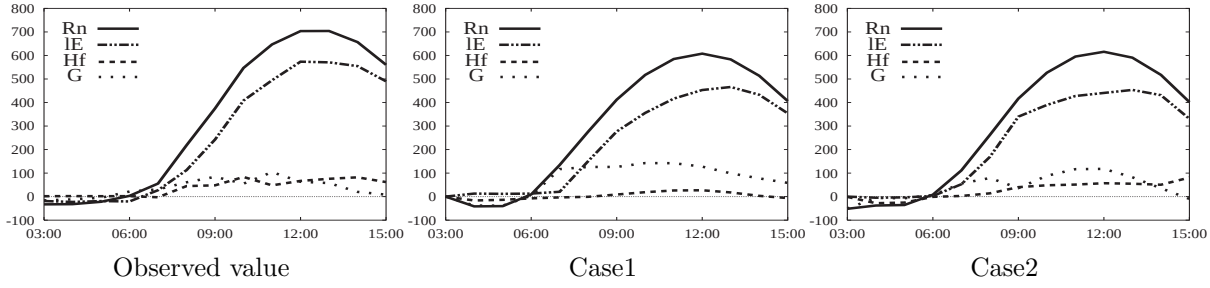

Fig. 4 Diurnal variation of surface energy balance at the paddy field site (W/m^2)
(Rn:net radiation, lE:latent heat, Hf:sensible heat, G:heat storage)

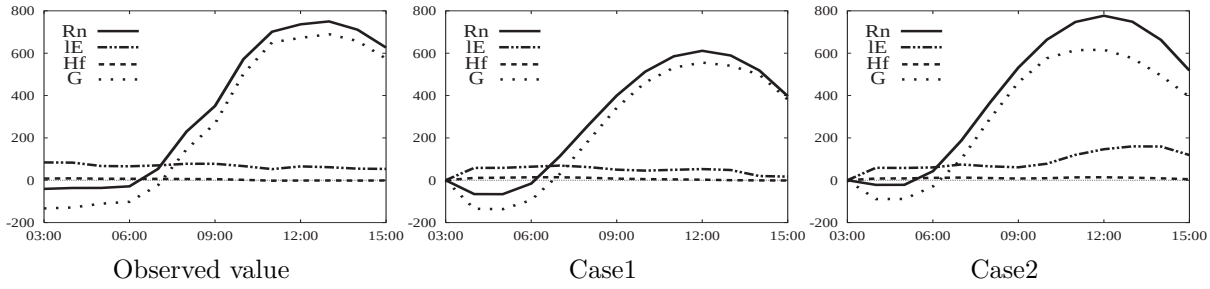

Fig. 5 Diurnal variation of surface energy balance at the lake site (W/m^2)

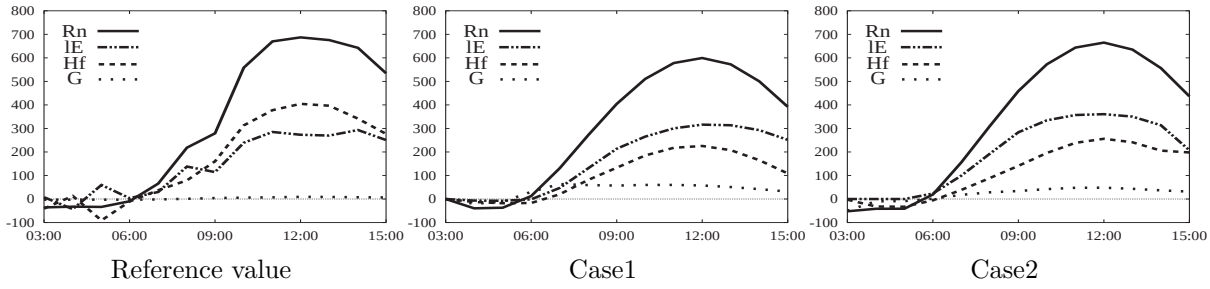

Fig. 6 Diurnal variation of surface energy balance at the forest site (W/m^2)
note : Reference flux data was obserbed on 24th August

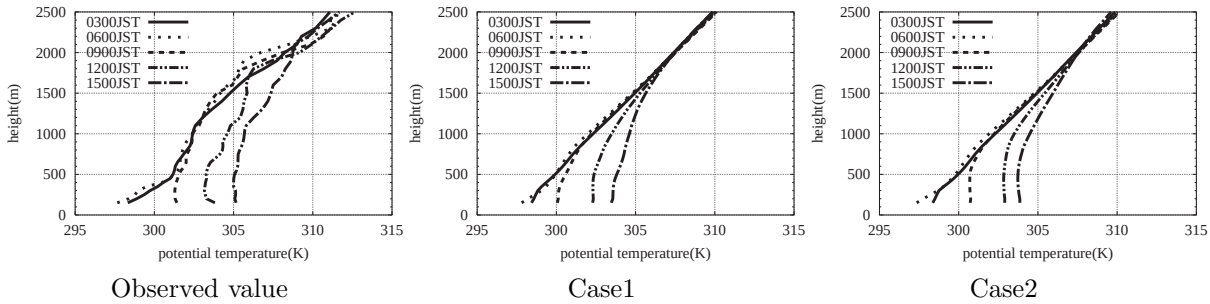

Fig. 7 Vertical profiles of potential temperature at different time on 14th August near the paddy field site

4.2 Local circulation within the basin

The left figure of Fig. 7 shows vertical profiles of potential temperature observed by radiosonde near the paddy field site. In this figure, two mixed layers can be seen at 12:00JST. First one is defined from surface to about 700m, where the profile of potential temperature shows almost neutral, and the other layer is defined from 700m to about 1800m, where potential temperature increases and vertical gradient becomes smaller than 09:00JST. According to Kimura and Kuwagata (1995), the lower mixed layer is caused by turbulent diffusion, whereas upper mixed layer is caused by heat transport with local circulation. An extended mixed layer, defined from surface to about 2000m, can be also seen at 15:00JST.

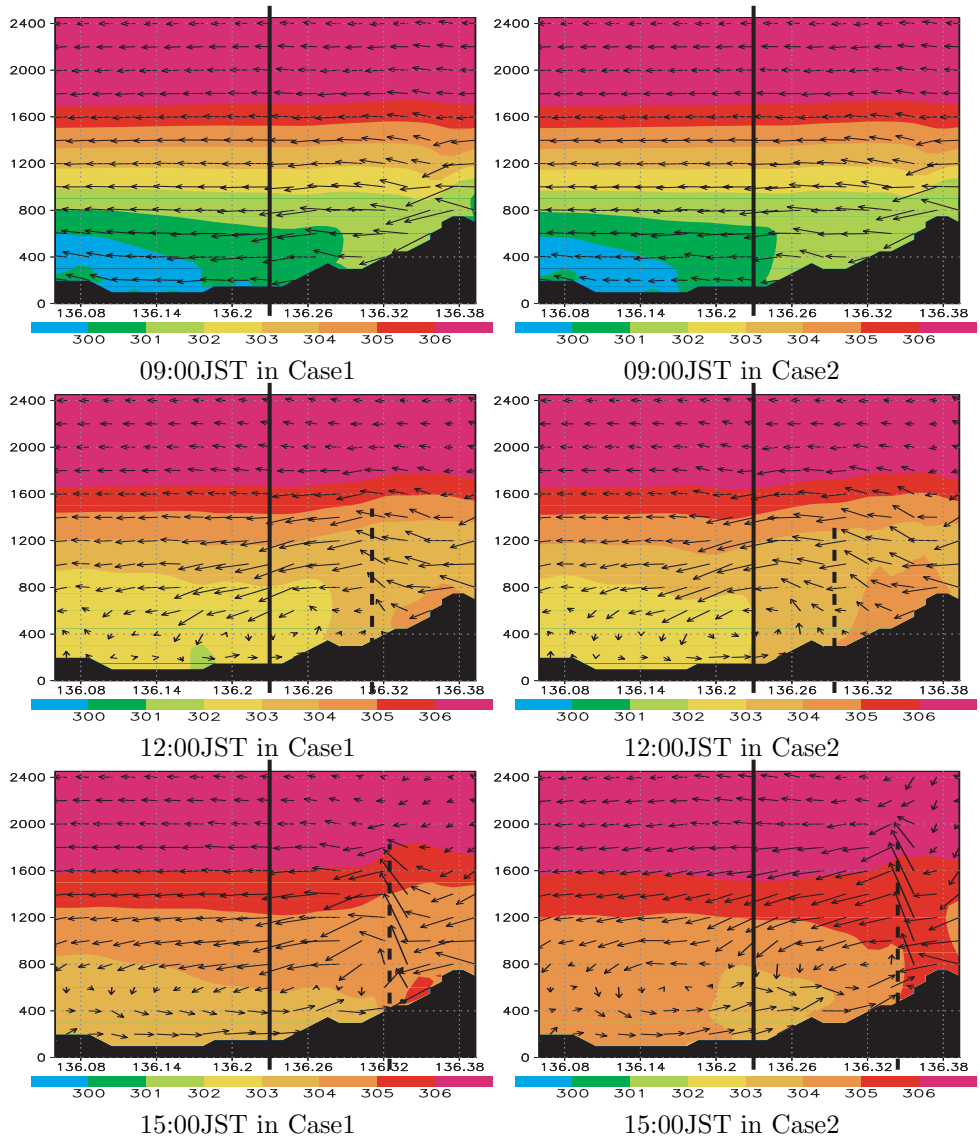

Fig. 8 East-west vertical cross section of potential temperature(K) and wind vector at the paddy field site. The solid lines indicate the position of vertical profile in Fig. 7. The dashed lines represent the positions of the lake breeze front

Fig. 7 shows that both Case1 and Case2 can simulate the feature found in observed vertical profiles of potential temperature qualitatively. The height of the mixed layer in Case1 and Case2 are about 1600m and 1800m, respectively, whereas the observed value is about 2000m. The height of the mixed layer in Case2 is better than Case1. This suggests that the amount of heat transportation from the eastern mountainous part to the valley bottom by the local circulation in Case2 is more than that in Case1. This may be explained that heat from land surface in Case2 is stronger than Case1, as described later. East-west vertical cross section of potential temperature and wind field is shown in Fig. 8. It can be seen that the potential temperature in Case2 is higher than Case1.

The wind direction data observed by AMeDAS station show that the lake breeze was well developed on the east shore of the Lake Biwa. However, the up-valley wind was not developed in the eastern mountainous part of the Lake Biwa Basin on 14th August. During the morning period, wind direction on the east shore of the Lake Biwa was east due to the Pacific high. In the afternoon period, the lake breeze developed, and wind direction was changed from east to west(see Fig. 9). And this

feature is schematically shown in Fig. 10.

It is shown in Fig. 8 that the development of the lake breeze and passing of the lake breeze front over the east shore of the Lake Biwa are simulated well by both Case1 and Case2. The change of wind direction on the east shore of the Lake Biwa simulated by both Case1 and Case2 are also shown in Fig. 9. Although the time when wind direction change from east to west presents an one-hour delay for both Case1 and Case2, both models can simulate the important feature of the lake breeze (changes of wind direction) relatively well.

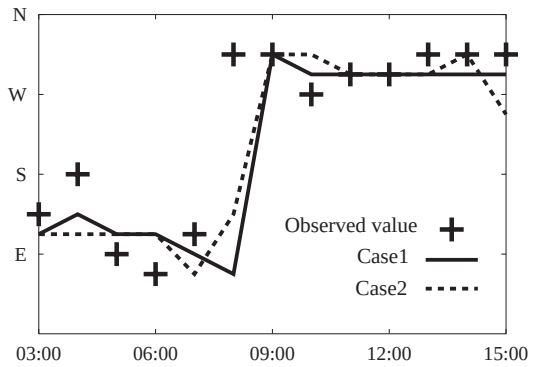

Fig. 9 Wind direction at the east shore of the Lake Biwa (Hikone)

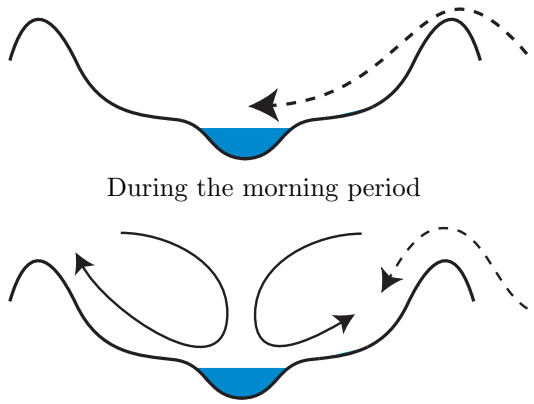

Fig. 10 Schematic image of the local circulation within the Lake Biwa Basin according to observed data

Near surface wind speed and air temperature are compared with observation at 8 points (see the right panel of Fig. 1), and root mean square errors of two experiments are listed in Table 3. We can see that the accuracy of temperature in Case2 is better than that in Case1.

Table 3 Accuracy of near-surface wind speed and air temperature at 8 points

	Case1	Case2
Wind speed(m/s)	1.0	0.9
Air temperature(K)	1.85	1.47

This may be explained as follows. Near surface temperature on the east shore of the Lake Biwa is underestimated in Case1 (see Fig. 8) by the weaker surface heating (sensible heat flux) than Case2.

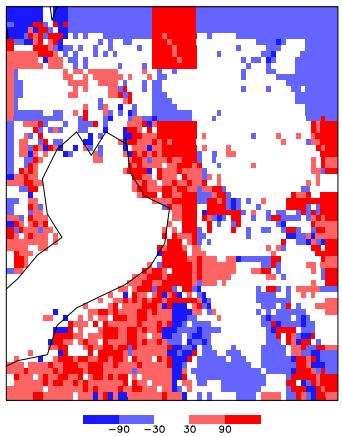

Fig. 11 Difference of sensible heat flux (Case2 - Case1) at 12:00JST on 14th August

Fig. 11 shows the difference of the sensible heat flux between Case2 and Case1. Although the coarse resolution of soil type dataset causes unrealistic horizontal distribution in the output of Case1 (ISBA predicts only one surface temterature, i.e. canopy and soil composite, and surface temperature is highly dependent upon the soil heat capacity), it can be seen that difference of the sensible heat flux is not seen on the lake and in the mountainous area (mostly forest). This agrees with the discussion about Fig. 5 and Fig. 6. On the other hand, sensible heat flux on the east shore of the Lake Biwa in Case2 is larger than Case1 .

Fig. 12 shows the fraction of urban area in each grid. The grids in which the fraction of urban area is large can be seen on the east shore of the Lake Biwa. In such grids, sensible heat flux is expected to be stronger than other grids. Fig. 13 shows the grids which are classified as cultivation in Case1 (dominant landcover is paddy field). Of

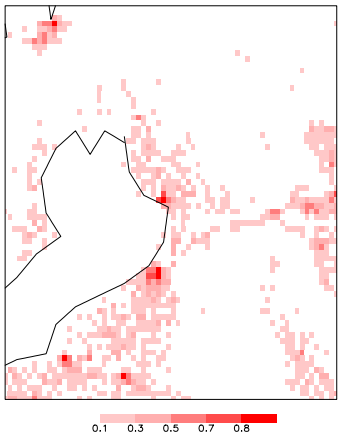

Fig. 12 Fraction of urban area in each grid

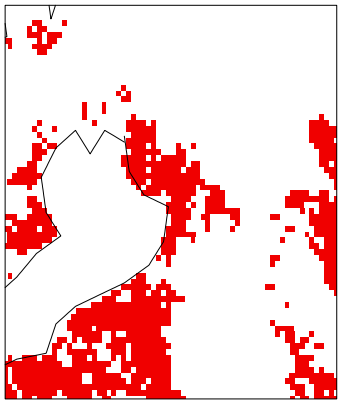

Fig. 13 The grids in which land uses are classified as cultivation in the ISBA model

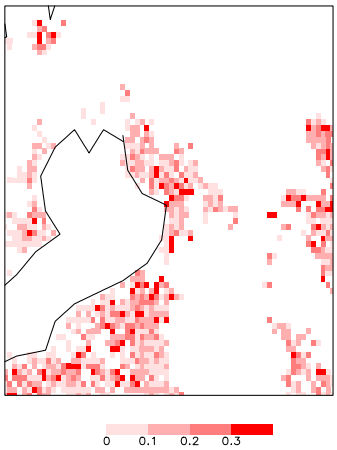

Fig. 14 The fractions of urban area in the grids shown in Fig. 13

course, the fraction of urban area in such grids is smaller than that of paddy field, but it still has a significant part (around 0.3) in some grids (see Fig. 14). The contributions of urban heating in such grids are omitted in Case1 (dominant landcover), but these are considered in Case2 (mosaic scheme). There are no evident difference between Case1 and Case2 in the results of surface energy balance at paddy field (see Fig. 4). Therefore, the increase in sensible heat flux in Case2 is explained by the contribution of sub-grid scale urban area. Turbulent diffusion is enhanced by the stronger sensible heat flux on the east shore of the Lake Biwa in Case2. Also, heat transport by local circulation is enhanced by larger difference of surface temperature between the lake and land surface in Case2. As a result, mosaic approach and urban canopy model of SiBUC can improve the development of local circulation and accuracy of near surface air temperature.

5. Numerical experiment for landcover change (Case3 & Case4)

5.1 Experimental design

Model domain for Case3 through Case6 (see Fig. 15) is different from Case1 and Case2. Fine resolution (1.5km) domain (step2: 148 × 148) is nested within coarse resolution (16km) domain (step1: 52 × 52). Other model configurations of ARPS are same as Case1 and Case2.

Simulation period is from 09:00JST to 18:00JST on 15th August 2001. It was a calm summer time sunny day, and whole Japan area was covered by the Pacific high. There was a thunderstorm event in the afternoon arizing from Hida and Kiso mountain range, and reaching to mountainous region in the north-east part of the Lake Biwa.

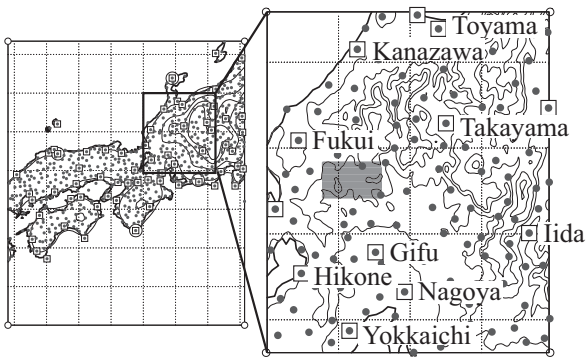

Fig. 15 Simulation domain for Case3 through Case6 (●:AMeDAS, □:SDP, ○:sonde)

In this section. the effects of water vapor flux (latent heat flux) and surface heating (sensible heat flux) on the distribution of rainfall are compared by replacing the landcover from forest to paddy field. This alteration will reduce the surface heating (weaken the local circulation) and increase the evaporation.

5.2 Definition of index used in discussion

Before move into discussion, some physical indices which are related to the status of atmosphere should be summarized for better understanding.

Precipitable Water (PW)

Precipitable water (PW) is defined as a total of water vapor exists in a air column with a unit area. Unit of PW is kg/m^2.

$$PW = \int_0^\infty \rho_w dz \quad \cdots\cdots\cdots\cdots\cdots\cdots \quad (1)$$

Here, ρ_w is a mass of water vapor in a unit volume of moist air.

Showalter Stability Index (SSI)

To quantify the stability of atmosphere, SSI(Showalter Stability Index) is used in this study. SSI is known to be a good index for the existence of lightning relevant to convective rain.

$$SSI = T_{500} - T_{850\to500} \quad \cdots\cdots\cdots\cdots\cdots\cdots \quad (2)$$

Here, T_{500} is a temperature at 500hPa level, and $T_{850\to500}$ is a temperature that will be obtained by uplifting dry-adiabatically the air mass at 850hPa level to condensation level, and further uplifting wet-adiabatically to 500hPa level. When the value of SSI is smaller, the atmosphere is more unstable (easier to produce convective rain). When the land surface is higher than 850hPa level, SSI cannot be defined.

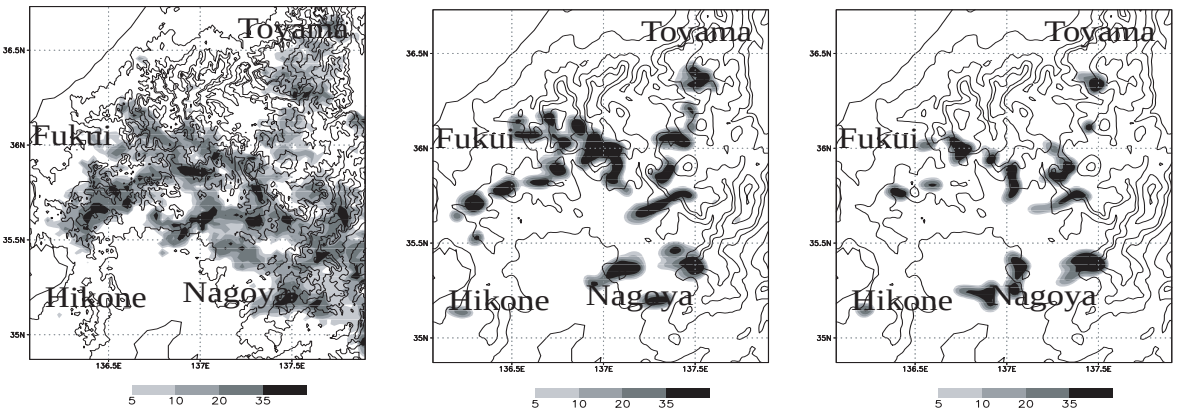

Observation(Rap) Case3 Case4

Fig. 16 6-hour total precipitation from 12:00JST to 18:00JST on 15th August

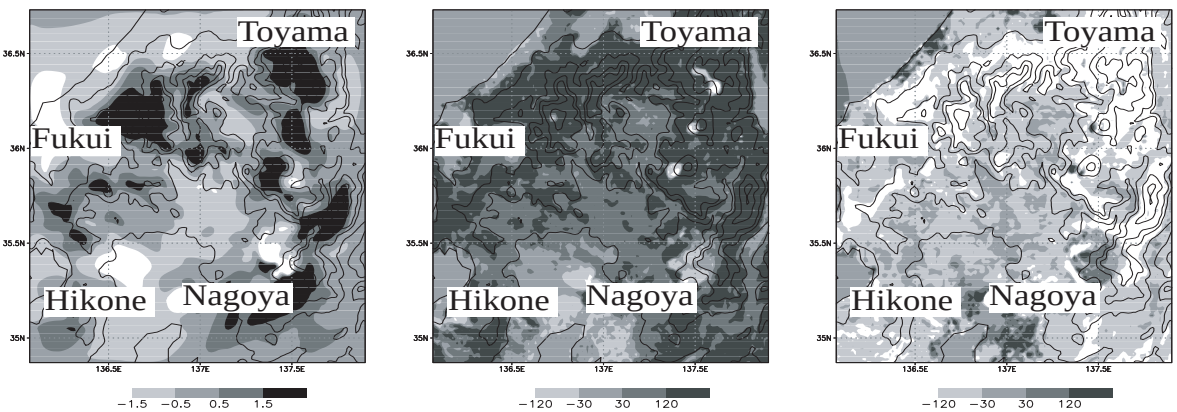

(a) Precipitable water (b) Sensible heat flux (c) Latent heat flux

Fig. 17 Difference between Case3 and Case4 (Case3-Case4) at 13:00JST

5.3 Results and discussion

6-hour total precipitation from 12:00JST to 18:00JST for both cases are shown in Fig. 16. And the differences between Case3 and Case4 for PW, sensible and latent heat fluxes are shown in Fig. 17. Rainfall amount in the mountaneous region located in the north-east part of the lake Biwa for Case4 is clearly reduced from Case3. As intended, the surface heating is reduced and evaporation is increased in Case4. Although the evaporation of Case4 is larger than Case3, the precipitable water in the mountaneous region is decreased.

Table 4 Change of PW from 09:00JST to 13:00JST and its source (kg/m^2) in Case3 and Case4

	Case3	Case4	difference
ΔPW	2.99	2.49	0.50
$Evap$	1.85	2.29	-0.44
$Conv$	1.14	0.20	0.94

The change of PW from initial time (09:00JST) to 13:00JST, total evaporation, and total water vapor convergence for that area (shaded area in the right panel of Fig. 15, hereafter, this area is called as Area M) are listed in Table 4. The reduction of water vapor convergence was larger than the increase of evaporation, and, as a result, the total precipitable water in Case4 was smaller than Case3. This result suggests that when the background atmosphere is wet enough (high PW), the surface heating and resulting water vapor convergence (water vapor transport) via local circulation is more important for the convective rain system than the supply of water vapor from surface evaporation. Fig. 18 shows the vertical profile (averaged over Area M) of specific humidity. In the lower levels (from 950 to 900hPa), specific humidity of Case4 is about 2g/kg larger than Case3 due to the intense surface evaporation. While, in the middle levels (900 to 750hPa), it is about 1.5g/kg smaller. And in the higher levels (above 750hPa), there is no difference between Case3 and Case4. In this way, the compensation mechanism of water vapor transport by the enhanced local circulation can be seen from Fig. 18. As a result, total water vapor in the lower to middle atmosphere for Case4 is smaller than Case3, and also temperature for Case4 is lower than Case3. Therefore, SSI for Case4 is higher than Case3 (see Fig. 19), and Case4, that is higher evaporation and smaller heating, was harder condition for convective rain.

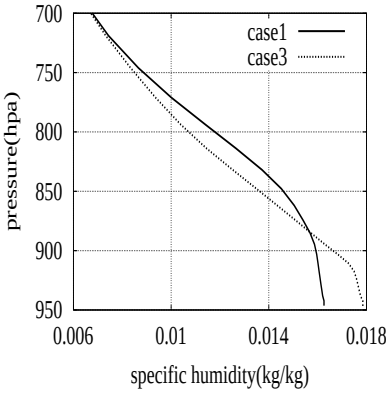

Fig. 18 Vertical profile of specific humidity (kg/kg) at 13:00JST for Case3 and case4

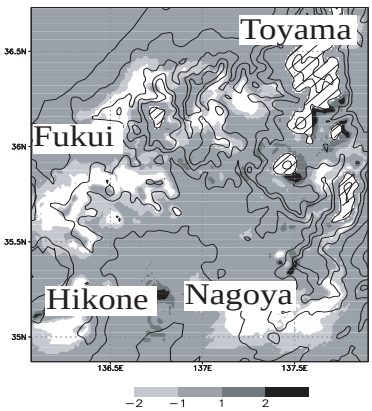

Fig. 19 Difference (Case3-Case4) of SSI(K) at 13:00JST : hatched area is undefined

6. Numerical experiment for soil wetness change (Case5 & Case6)

6.1 Experimental design

In this section, effects of soil wetness on the distribution and the amount of rainfall are investigated by replacing the initial soil wetness from wet condition to dry condition. Simulation period and model domain are same as those of Case3 and Case4. As a numerical experiment for investigating the sensitivity to soil wetness, any condition can be used for dry run. For example, extremely dry condition that can be seen in the arid or semi-arid area can be used for dry case. Here, more

realistic (or possible) case is selected to see how the actual time-space variability of soil moisture can affect the results of the short-term weather prediction in humid temperate climate condition like Japan.

Time series of matric potential observed at the forest site in August 2001 is shown in Fig. 20. The original data were obtained as volumetric soil moisture by TDR sensor installed between 10cm and 30cm depth. Using the soil physical properties for sandy clay and $\theta - \psi$ relationship of Clapp and Hornberger, volumetric soil moisture data were converted into matric potential.

In the mountain area (mostly covered with forest), vegetation coverage is high, and surface energy balance is mainly dependent on the intensity of transpiration which is highly controlled by the root-zone soil moisture. In the SiBUC model, the physiological parameters to express the stress of soil moisture for calculating canopy resistance are given by matric potential (ψ_{c1}, ψ_{c2}: leaf water potential at which leaf stomata start to close, completely close). That is why time series of soil moisture (Fig. 20) is expressed in matric potential.

According to Fig. 20, matric potential at the forest site had its minimum (ψ = -130m) on 21st August. This condition is selected as dry case (Case6). As for wet case (Case5), the value at field capacity (ψ = -0.63m) which can be seen just after rainfall event is selected. Considering that the summer of 2001 was not so dry, these two conditions are regarded to be within realistic range.

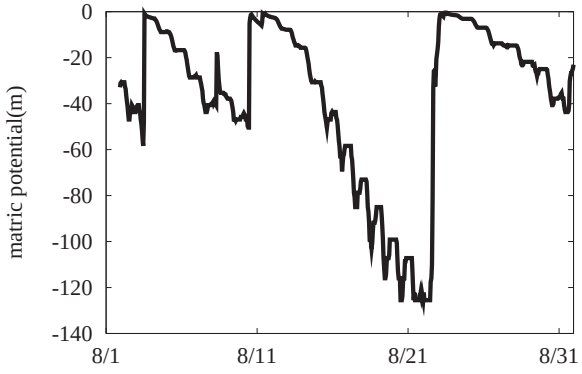

Fig. 20 Time series of observed matric potential at forest site in August 2001

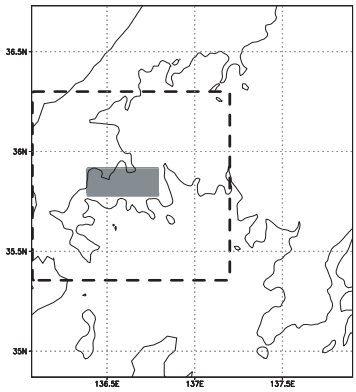

Fig. 21 Analysis domains discussed in Section 6 (box with broken line) and Table 5 (shaded box)

6.2 Results and discussion

In this section, the analysis is focuced on the north-east part of the lake Biwa (shown by the box with broken line in Fig. 21) where typical thunderstorm event was observed.

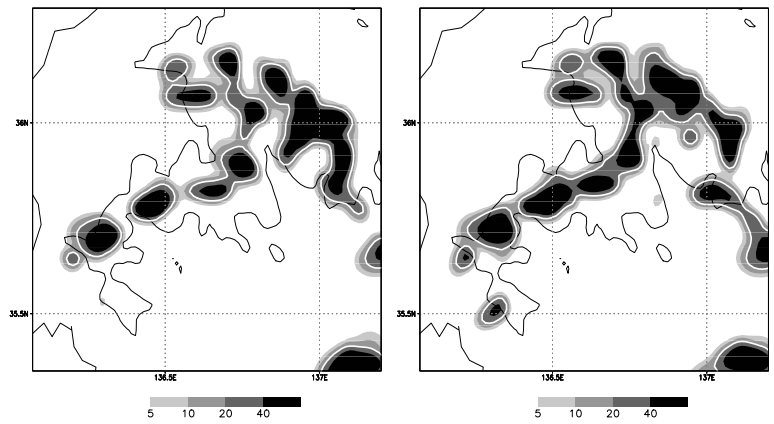

(a) Case5 (wet) (b) Case6 (dry)

Fig. 22 6-hour total precipitation from 12:00JST to 18:00JST on 15th August with wet and dry condition. The white thick line indicates accumulated rainfall of 20 mm.

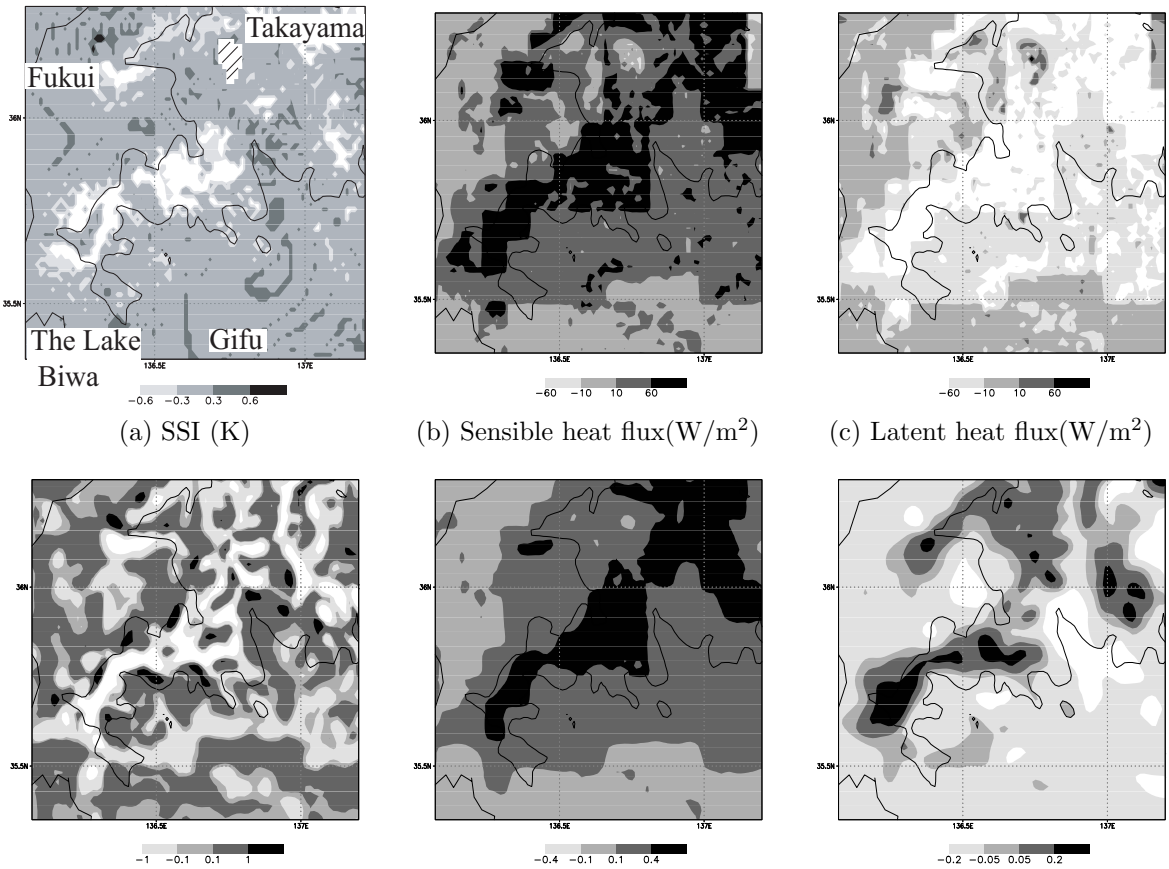

(a) SSI (K) (b) Sensible heat flux(W/m^2) (c) Latent heat flux(W/m^2)

(d) Divergence (10^{-4}/s) (e) Potential Temperature(K) (f) Precipitable water (kg/m^2)

Fig. 23 The difference between Case5 and Case6 (Case6-Case5) at 12:00JST

6-hour total precipitation from 12:00JST to 18:00JST for both cases are shown in Fig. 22. The area where there is more than 20mm rainfall (white thick line in Fig. 22) for Case6 (dry) is clearly larger than that for Case5 (wet). This result suggests that the soil moisture difference within a realistic variation range in the humid climate condition does affect the amount of summer convective rainfall even in a very short-term prediction (several hours).

The differences between Case5 and Case6 (Case6-Case5) at 12:00JST for SSI, sensible and latent heat fluxes, divergence, potential temperature, and PW are shown in Fig. 23. As expected, the surface heating is larger and evaporation is smaller in Case6 (see Fig. 23(b),(c)). This means that soil moisture condition in Case6 is dry enough to regulate evapotranspiration. Although the evaporation of Case6 is smaller than Case5, PW is increased in the dry case (Fig. 23(f)). Potential temperature is also higher in Case6 (Fig. 23(e)). As a results, SSI for Case6 is smaller (unstable) than Case5. These features are same as those of Case3 and Case4.

Table 5 Change of PW from 09:00JST to 13:00JST and its source (kg/m^2) in Case5 and Case6

	Case5	Case6	difference
ΔPW	1.76	1.83	0.07
$Evap$	1.34	1.14	-0.20
$Conv$	0.42	0.69	0.27

In the same way as Table 4, the change of PW from initial time to 12:00JST, total evaporation, and total water vapor convergence are listed in Table 5. The increase of water vapor convergence was larger than the decrease of evaporation in dry case, and, as a result, the total precipitable water in Case6 was larger than Case5. Although the absolute values in Table 5 are smaller than Table 4, the compensation mechanism of water vapor transport by the enhanced local circulation does exist in this soil wetness change experiment.

7. Conclusion

In this study, six numerical experiments are carried out in mountainous region around the Lake Biwa on 14th and 15th August in 2001. The results of the LSS change experiments (Case1 & Case2) indicate that detailed treatment of land cover condition, especially, the inclusion of sub-grid scale contribution of urban heating could improve the development of local circulation. The results of the land cover change experiments (Case3 & Case4) suggest that when the background atmosphere is wet enough, the surface heating is more important for the convective rain system than surface evaporation. The results of the soil wetness change experiments (Case5 & Case6) suggest that the soil moisture difference within a realistic range in the humid climate condition does affect the amount of summer convective rainfall even in a very short-term prediction.

Acknowledgements

This research is supported by the grant for science and technology (A)(1)13305033 and COE(Center Of Excellence) program of DPRI, Kyoto University. The Advanced Regional Prediction System (ARPS), which has been developed by the CAPS, Unversity of Oklahoma is used. Authors are grateful to the Dr. Nobuhiro Ebisu (Ehime University) for providing the observation data at the forest site.

References

Kanae, S., Oki,T., and Musiake,K. (2001) : Impact of Deforestation on Regional Precipitation over the Indochina Peninsula, J. Hydrometeor., 2, pp.51-70.

Kimura,F. and Kuwagata,T. (1995) : Horizontal heat fluxes over complex terrain computed using a simple mixed-layer model and a numerical model, J. Appl. Meteor., pp.549-558.

Koster,R.D., Dirmeyer,P.A., and others (2004) : Regions of Strong Coupling Between Soil Moisture and Precipitation, Science, Aug, 2004, pp.1138-1140.

Noilhan,J. and Planton,S. (1989) : A simple parameterization of land surface processes for meteorological models, Mon. Wea. Rev., 117, pp.536-549.

Sellers,P.J., and others (1986) : A simple biosphere model(SiB) for use within general circulation models, J. Atmos. Sci., 43, pp.505-531.

Shinoda,T. and Uyeda,H. (2002) : Effective Factors in the Development of Deep Convective Clouds over the Wet Region of Eastern China during the Summer Monsoon Season, J. Meteor. Soc. Japan, 80-6, pp.1395-1414.

Tanaka,K., Nakakita,E., and Ikebuchi,S. (1998) : Land-surface Parameterization in the Lake Biwa Project, Annual Journal of Hydraulic Engineering, JSCE, 42, pp.79-84 (in Japanese).

Xue,M., Droegemeier,K.K., and others (1995) : Advanced Regional Prediction System (ARPS) Version 4.0 User's Guide.

短時間数値気象予測における地表面加熱の重要性

田中賢治 · 相馬一義 * · 中北英一 · 池淵周一

* 京都大学工学研究科

要 旨

本研究では、夏季の対流性降雨の発生に対する地表面加熱や土壌水分状態の重要性を調べることを目的として、2001 年 8 月 14 日と 15 日の事例に関して琵琶湖周辺の山岳域を対象に 6 つの数値実験が実行された。その結果、地表面条件（土地利用、サブグリッドの都市の効果）や土壌水分状態は非常に短期間の数値予報においても対流性降雨に影響を与えることが示された。

キーワード：土地利用，土壌水分，局地循環，対流性降水，短時間予測